ADVANCED FUNCTIONAL MATERIALS
www.afm-journal.de

Novel Color Converters for High Brightness Laser-Driven Projection Display: Transparent Ceramics–Glass Ceramics Film Composite

Shengxiang Liao, Shilin Jin, Tao Pang, Shisheng Lin, Yuanhui Zheng, Ronghua Chen, Guoyu Xi, Xiaoyan Li,* Bin Zhuang, Feng Huang, and Daqin Chen**

Laser-driven projection display puts forward urgent demand for color converter materials to simultaneously achieve balanced-spectrum properties and strong heat dissipation. Herein, this work develops a novel optofunctional composite by coupling $Y_3Al_5O_{12}:Ce^{3+}$ transparent ceramics (TC) with $CaAlSiN_3:Eu^{2+}$ phosphor-in-glass film (PiGF) for the first time. Remarkably, this new material architecture design enables a balance between the spectrum properties and heat dissipation ability, and can yield high-quality white light with brightness of over 2500 lm, luminous efficacy (LE) of over 200 lm W^{-1}, correlated color temperature (CCT) of 3700–4100 K, and improved color rendering index (CRI) of 60–70. Furthermore, the PiGF@TC-converted laser projection system is also successfully designed, showing natural and real color restoration. Additionally, the combined action of thermal quenching and optical excitation intensity quenching is confirmed for the luminescence saturation upon high-power blue laser driven. The main mechanism of optical quenching is identified to be energy upconversion dominated by second-order nonlinear processes. The findings described here suggest a step toward developing the admirable laser-driven color converters for next-generation lighting sources.

1. Introduction

At present, lighting sources are developing toward higher brightness and more energy saving. However, under high input electric power, white light-emitting diode (LED) is suffering from the notorious problem of "efficiency droop".[1] Although integrated multichips or multilamps can be applied to improve the brightness of white LED, it still brings about a series of new issues, such as increased cost, stability reduction, light efficiency sacrifice, and complex lamp design.[2] In lieu of LED, laser diode (LD) has been extensively explored for its more stable wall plug efficiency, brighter luminescence per chip area, and higher directionality.[3]

In terms of projection display, the lighting source based on the combination of blue LD with broadband-emission color converters is the most common technology.[3b,4] Even the up-to-date

S. Liao, S. Jin, R. Chen, G. Xi, B. Zhuang, F. Huang, D. Chen
College of Physics and Energy
Fujian Normal University
Fuzhou, Fujian 350117, P. R. China
E-mail: dqchen@fjnu.edu.cn

T. Pang
Huzhou Key Laboratory of Materials for Energy Conversion and Storage
College of Science
Huzhou University
Zhejiang, Huzhou 313000, China

S. Lin, D. Chen
Fujian Provincial Collaborative Innovation Center for Advanced High-Field Superconducting Materials and Engineering
Fujian Normal University
Fuzhou, Fujian 350117, P. R. China
E-mail: linshisheng@fjirsm.ac.cn

S. Lin, D. Chen
Fujian Provincial Engineering Technology Research Center of Solar Energy Conversion and Energy Storage
Fujian Normal University
Fuzhou, Fujian 350117, P. R. China

S. Lin
Key Laboratory of Optoelectronic Materials Chemistry and Physics
Fujian Institute of Research on the Structure of Matter
Chinese Academy of Sciences
Fuzhou 350002, P. R. China

Y. Zheng, D. Chen
Fujian Science & Technology Innovation Laboratory for Optoelectronic Information
Fuzhou, Fujian 350116, P. R. China

Y. Zheng
College of Chemistry
Fuzhou University
Fuzhou, Fujian 350116, P. R. China

The ORCID identification number(s) for the author(s) of this article can be found under https://doi.org/10.1002/adfm.202307761

DOI: 10.1002/adfm.202307761

Table 1. The achieved optical performance of phosphor ceramics, phosphor in glass and PiGF@TC (TC is transparent ceramics) composite upon high-power blue laser diode (LD) irradiation.

Phosphor converters	Chemical composition	Test mode	Excitation power [W]	Luminous flux [lm]	Luminous efficacy [lm W^{-1}]	Luminance saturation [W mm^{-2}]	Thermal conductivity [W $(m \times K)^{-1}$]	Refs.
Phosphor ceramics	YAG:Ce^{3+}	Static/transmission	6.00	739.8	123.3	12.00	10.20	[14]
	LuAG:Ce^{3+}	Static/transmission	8.50	1203.6	141.6	15.20	7.60	[15]
	CASN:Eu^{2+}	Static/transmission	4.74	≈200	42.2	1.50	4.20	[16]
Phosphor in glass	LuAG:Ce^{3+}	Static/all	2.93	634.46	216.4	3.73	4.95	[17]
	YAGG:Ce^{3+}	Static/all	2.18	555.6	254.5	2.78	1.71	[18]
	CASN:Eu^{2+}	Static/reflection	–	49.27	–	1.90	–	[19]
	β-Sialon:Eu^{2+}	Static/all	2.36	363	154.0	4.02	4.62	[20]
	$Mg_2Al_4Si_5O_{18}$:Eu^{2+}	Static/reflection	5.07	274	54.0	3.25	2.20	[21]
PiGF@TC	CASN:Eu PiGF–YAG:Ce TC	Static/reflection	18.00	3935	218.6	7.08	10.33	This work

"all" means containing both transmissive light and reflective light.

commercial laser-driven projection display is based on directly making broadband-spectra light as backlight or filtering the broadband-spectra light into R/G/B/Y primary colors.[5] The first demonstration of using broadband-emission phosphor driven by blue laser for projection display is proposed by Texas Instruments. Thereafter, Appotronics (ALPD1.0, ALPD2.0, ALPD3.0, and ALPD4.0), Sony (VPL-GTZ380), and Maxell (MMP-J4001U) demonstrated the validity of this strategy in the other architecture systems. One great advantage of the usage of broadband-emission color converters is high luminance output, due to its excellent luminescence saturation performance upon high-power blue laser driven. Although narrow emitting band color converter can help improve the color gamut to some extent, its LE upon blue laser driven (<100 lm W^{-1}) is still far from satisfying the demand for application in high brightness laser-driven projection display.[3a,4a] Therefore, their application in laser-driven projection display is just proof-of-concept experiment for now.

It is worth noting that irradiated with ultra-high power density, color converters are subjecting to the loss of irradiation transitions and the thermal effects from blue LD, which puts forward stringent requirements on their optical performance and heat dissipation.[6] Among various broadband-emission yellow-emitting color converters, $Y_3Al_5O_{12}$:Ce^{3+} (YAG:Ce) is the core material that cannot be replaced, and extensive research has been conducted on fabricating into different forms of YAG, such as phosphor-in-silicone,[7] single crystal,[8] glass ceramic,[9] glass ceramic film,[10] and TC.[11] Among them, the TC is obviously the most suitable for laser colorconverters, with its high thermal conductivity, strong irradiation resistance, and superior emitting light quality.

Nevertheless, the deficiency of red emissive component significantly affects the practical application of YAG:Ce TC, negatively affecting the achievable performance of the constructed projection display. In general, there are two ways to realize the spectral compensation of YAG:Ce TC: modifying host and luminescence center regulation. The former one is to replace the corresponding sites of YAG by Ga^{3+}, Gd^{3+}, Sc^{3+}, Mg^{2+}, and Si^{4+} for realizing the modify of crystal-field splitting.[12] The latter is to use codoped red-emitting activators, such as Pr^{3+}, Mn^{2+}, or $Cr.^{3+}$[13] Although the two approaches have achieved success to some extent, intrinsic limitations still exist, including inducing impurity phase, increasing porosity, and decreasing efficiency.

As such, in this study, a new material architecture design of "ceramic + glass ceramic film" was proposed for the first time, to develop color converters potentially applicable to laser-driven projection display. This design aims to make highly efficient $CaAlSiN_3$:Eu^{2+} (CASN:Eu) red phosphor and low-melting glass cosintered on TC to simultaneously achieve the balanced-spectrum properties and strong heat dissipation. Based on this design, we explored a novel type of color converter, i.e., CASN:Eu PiGF–YAG:Ce TC composite (PiGF@TC). Here, YAG:Ce TC can be used as both luminescent component and high thermal conductivity substrate. The results show that the developed composite has high thermal conductivity of 10.33 W m^{-1} K^{-1}, and meanwhile the introduce of CASN:Eu PiGF effectively solves the problem of deficient red emissive component upon the irradiation of blue LD. The constructed PiGF@TC-based lighting source yields luminosity-chromaticity balanced white light with brightness of over 2500 lm, LE of over 200 lm W^{-1}, CCT of 3700–4100 K, and improved CRI of 60–70. Compared with the traditional YAG:Ce TC-converted one, the constructed CASN:Eu PiGF–YAG:Ce TC-converted laser projection system shows better display performance. As tabulated in **Table 1**, it is found that PiGF@TC combines the merits of admirable luminescent performance and ultrahigh thermal conductivity from TC, as well as those of flexible composition design, and controllable chromaticity inherited from glass ceramic.

X. Li
Organic Optoelectronics Engineering Research Center of Fujian's Universities
College of Electronics and Information Science
Fujian Jiangxia University
Fuzhou 350108, China
E-mail: xyli@fjjxu.edu.cn

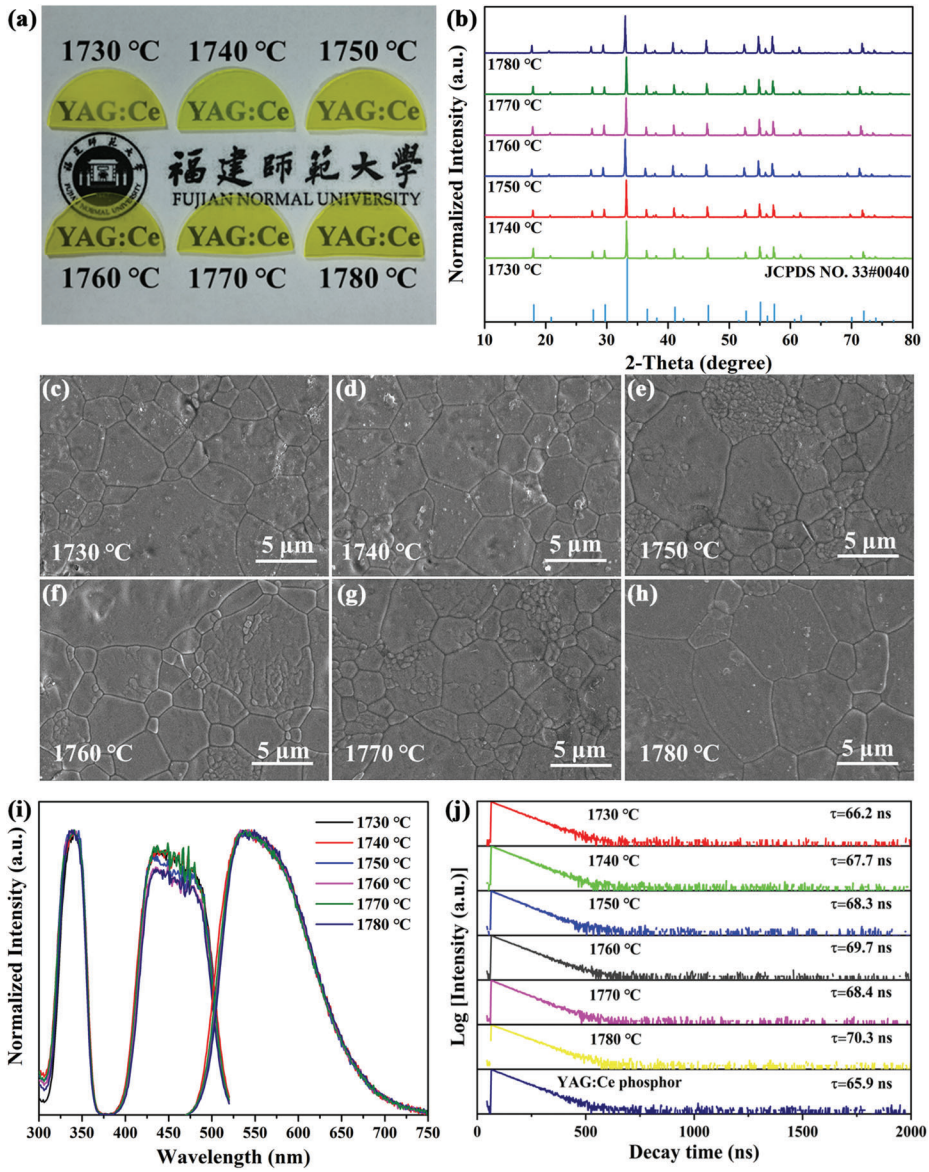

Figure 1. a) Photographs, b) X-ray diffraction (XRD) patterns, c–h) Scanning electron microscopy (SEM) images, i) Photoluminescence (PL)/PL excitation (PLE) spectra and j) PL decay curves of YAG:Ce transparent ceramics (TCs) prepared with different sintering temperatures.

2. Results and Discussion

YAG:Ce TCs were prepared by high temperature solid-state reaction under vacuum environment. The detailed preparation procedure was schematically illustrated in Figure S1 (Supporting Information). When thermally annealed at >1600 °C, Al_2O_3 and Y_2O_3 will fully solid-state react to form $Y_3Al_5O_{12}$ phase.[22] Nevertheless, in order to obtain YAG:Ce TC, it is very important to adjust the sintering parameters to achieve the controlled growth of grains. As such, YAG:Ce TCs sintered at various temperatures were fabricated. The appearance of these samples is displayed in **Figure 1**a. It can be seen that the body color is yellow, but the transparency is slightly different. As the sintering temperature elevates from 1730 °C to 1780 °C, the sample transparency gradually augments from 79.7%@800 nm to 93.2%@800 nm (Figure S2, Supporting Information). The corresponding X-ray diffraction (XRD) peaks are all identical to cubic $Y_3Al_5O_{12}$ (JCPDS No. 33–0040), indicating that no obvious impurity phases are detected (Figure 1b). It can also be seen that the XRD peaks of $Y_3Al_5O_{12}$ slightly shift toward low θ side compared with the standard card because of lattice expansion from introducing larger Ce^{3+} ion (r = 0. 1143 nm) to substitute Y^{3+} (r = 0.1019 nm) (Figure S3, Supporting Information). From scanning electron microscopy (SEM) observation, microparticles with closely arrangement, clear boundaries and irregular grain shapes can be clearly distinguished (Figure 3c–h). When the sintering temperature is 1730–1740 °C, some visible inner pores ≈0.5 μm acting as the scattering centers reduce the transparency. With the sintering temperature further elevates, good transparency is achieved because of the absence of these pores and the increase of grain size,

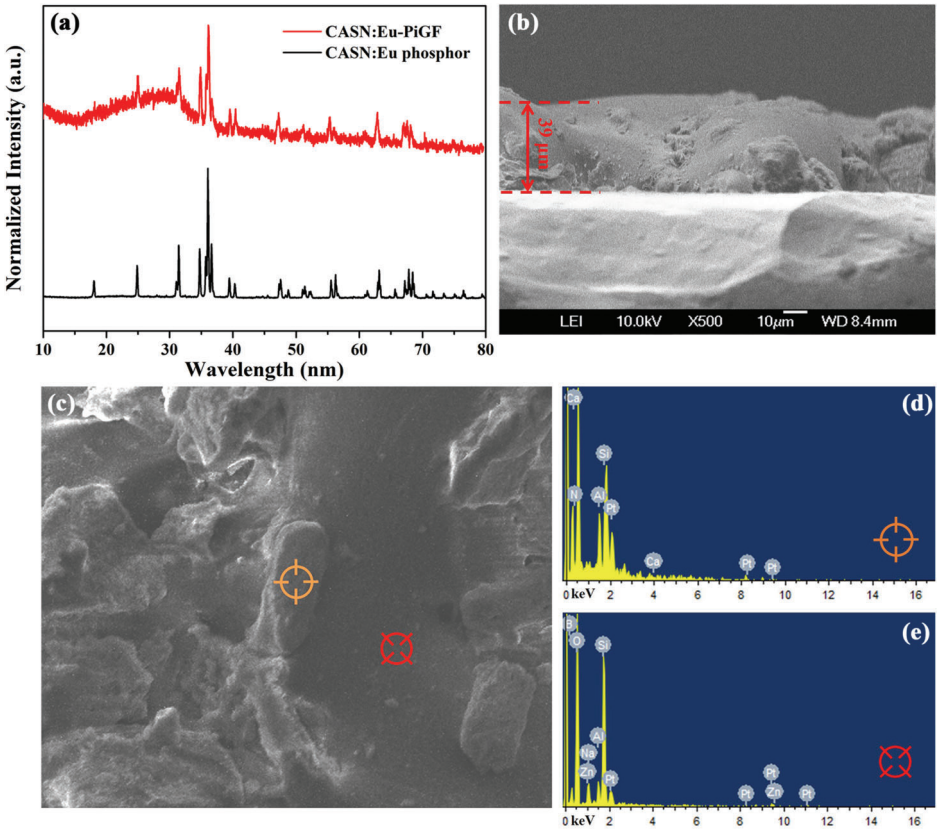

Figure 2. a) X-ray diffraction (XRD) patterns of CASN:Eu phosphor and CASN:Eu PiGF. Scanning electron microscopy (SEM) observation on the b) side view and c) enlarged region of CASN:Eu PiGF–YAG:Ce transparent ceramics (TC). Energy dispersive spectroscopy (EDS) spot analyses of d) a single phosphor particle and e) the glass matrix.

indicating that the increased sintering temperature can promote the growth of grain and the densification of ceramics. Energy dispersive spectroscopy (EDS) measurements demonstrate uniform distribution of Y, Al, O, and Ce elements (Figure S4, Supporting Information).

Subsequently, optical properties of YAG:Ce TC were investigated. All the TCs show broad photoluminescence (PL) at ≈540 nm with full width at half-maximum (FWHM) of ≈120 nm and two typical PL excitation (PLE) bands at 345 and 450 nm originated from Ce^{3+}:4f↔5d parity-allowed transitions (Figure 1i).[2c] Likewise, the kinetic luminescent decays of YAG:Ce TCs are all close to that of commercial YAG:Ce phosphors (≈65 ns) (Figure 1j), and the PL quantum yields (PLQYs) of YAG:Ce TCs can all reach ≈95% (Figure S5, Supporting Information). It is also worth noting that high-power laser irradiation will generally lead to thermal aggregation and weakened luminescence performance, indicating the vital importance of laser color converters' ability to resist thermal quenching. In Figure S6 (Supporting Information), the temperature-dependent PL spectra show that YAG:Ce TC has better thermal quenching resistance than commercial YAG:Ce phosphor powder, because the high thermal conductivity of TC helps to subsequently reduce the probability of the Ce^{3+} nonradiative transition. Considering phase identification, microstructure, and luminescence properties, the sintering temperature is optimized to 1780 °C for the present YAG:Ce TCs.

To address the issue of deficiency of red emissive component in YAG:Ce TC, a new material architecture of "CASN:Eu PiGF–YAG:Ce TC composite" is designed by cosintering CASN:Eu red phosphor and low-melting glass on TC (Figure S1, Supporting Information). PL spectra, PLE spectra, kinetic luminescent decay curves, and PLQYs of YAG:Ce TC before/after second sintering were tested and compared (Figure S7, Supporting Information). Evidently, no obvious change is detected after sintering at 680 °C for 30 min, confirming that mild second sintering has no significant effect on the optical performance of YAG:Ce TC. This provides the possibility for the combination of ceramics and glass ceramics film. After knife-coating the paste-like slurry, expelling organic solvents, and sintering, the CASN:Eu PiGF–YAG:Ce TC composite was obtained (Figure S1, Supporting Information). XRD pattern of CASN:Eu PiGF exhibits characteristic diffraction peaks of phosphor counterpart and an additional amorphous hump from the glass matrix (**Figure 2**a). SEM observation on cross-section of PiGF@TC shows that the CASN:Eu PiGF layer with thickness of 39 μm is tightly bonded to YAG:Ce TC (Figure 2b), verifying good film-forming ability. There is well-defined boundary between the CASN:Eu PiGF layer and YAG:Ce TC, indicating that PiGF will not react with the TC substrate. Compared with the pristine phosphor powders (Figure S8, Supporting Information), the morphology and size of the embedded CASN:Eu particles have not been significantly altered, indicating that the glass matrix have no erosion effect on the CASN:Eu

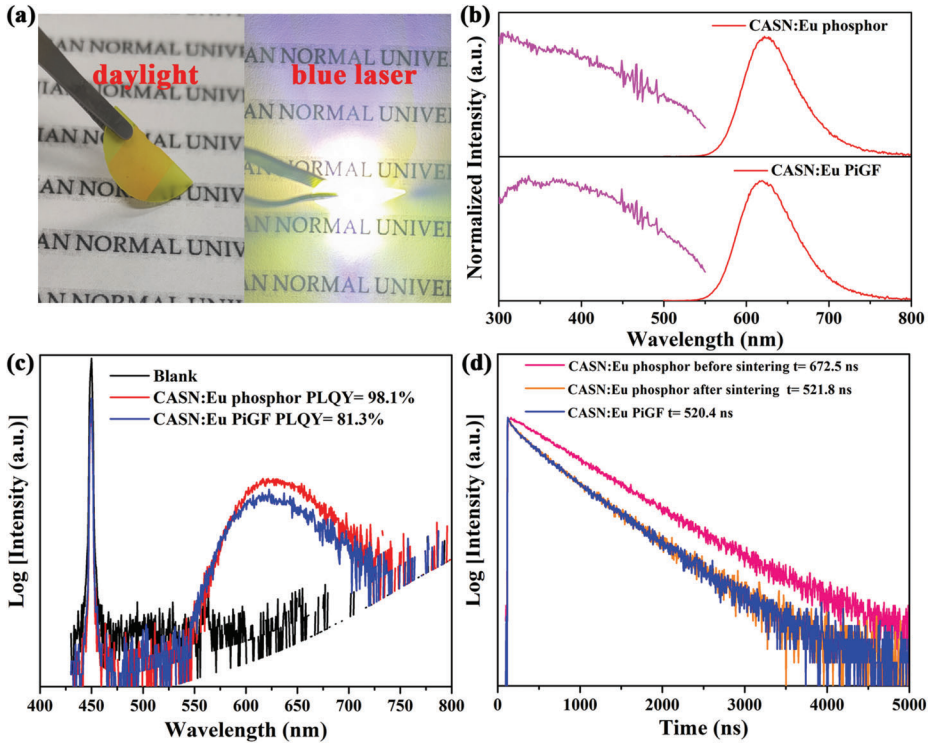

Figure 3. a) Appearance of the CASN:Eu PiGF–YAG:Ce transparent ceramics (TC) sample under daylight and blue laser irradiation. Comparison of b) photoluminescence (PL)/PL excitation (PLE) spectra, c) measured emission spectra to calculate PL quantum yields (PLQYs) under 450 nm blue light excitation and d) luminescent decay curves of CASN:Eu phosphor and CASN:Eu PiGF.

phosphor (Figure 2c). Based on the EDS point analysis (Figure 2d,e), one embedded particle and glass matrix are distinct and their respective chemical compositions, i.e., Ca, Al, Si, and N for the former one, and Si, B, Zn, Na, Al, and O for the latter one are detected. It is concluded that a novel composite color converter, CASN:Eu PiGF–YAG:Ce TC, is successfully fabricated by the proposed strategy of "ceramic + glass ceramic film."

The luminescent properties of CASN:Eu phosphor and the corresponding CASN:Eu PiGF were compared. It can be found that the spectral profile and position of CASN:Eu phosphor and PiGF are basically same, both of which have efficient red PL at ≈625 nm, and can be efficiently excited by blue light, ensuring excellent luminescent properties of CASN:Eu PiGF–YAG:Ce TC under blue laser driven (**Figure 3**a,b). After cosintering, PLQY of CASN:Eu PiGF shows slight decrease related to that of CASN:Eu phosphor, which can still reach as high as 81.3% (Figure 3c). As evidenced in Figure 3d, the decay lifetime of CASN:Eu phosphor decreases from 672.5 to 521.8 ns after sintering. Combined with the result of CASN:Eu PiGF (lifetime: 520.4 ns), it can be deduced that the thermal degradation of CASN:Eu in itself is the main reason for the lifetime alternation (Figure 3d). As the temperature increases, the integrated emission intensities of CASN:Eu PiGF exhibit superior thermal stabilities, with luminescent losses lower than 13.0% and 20.0% intensity of room temperature at 150 °C and 200 °C, respectively, benefiting from the rigid crystal structure of CASN:Eu (Figure S9, Supporting Information).

The luminous performance upon blue laser driven was measured in a self-built system composed of 50 W 450 nm blue laser, integrating sphere, fiber spectrometer, laser power meter, and infrared thermal imaging camera. The light path was firstly researched because it is significant to achieve performance of color converters upon blue laser irradiation (**Figure 4**a). Upon excitation in the transmission light path configuration, since a large amount of converted emission would be backward, "one-dimensional photonic crystals (1DPCs)" coated sapphire consisting of blue-light anti-reflection (AR) layer on one side and blue-light band-pass (BP) filter layer on the other side is considered to be introduced.[10b] As shown from the transmittance spectrum of AR-BP 1DPCs film coated sapphire (Jiangsu Optocera Optoelectronics Co., Ltd., China, Figure S10, Supporting Information), there is high transmittance in the blue light band, while the other types of light are all reflected to direct more blue light to excite color converters and to guide emission from backward to forward. In the reflection light path configuration, the composite material is mounted on Al plate with high thermal capacity. Electroluminescence (EL) spectra modified with three different configurations were recorded, as shown in Figure 4b. In line with our expectation, 1DPCs coated sapphire attached to the sample yields higher luminous flux (LF) of 159 lm @ 1.0 W than that of sample without 1DPCs (95 lm @ 1.0 W). The luminous performance in reflection mode is the best, with the LF even reaching 317 lm @ 1.0 W, due to the absence of lighting loss from backward. Meanwhile, the corresponding LE is consistent with the LF (Figure S11, Supporting Information). The plots of power density dependent LF (Figure 4c) also show that the reflection light path configuration has the maximal LF of 5478 lm. With the gradual increase of the input blue laser power, although the result of transmission

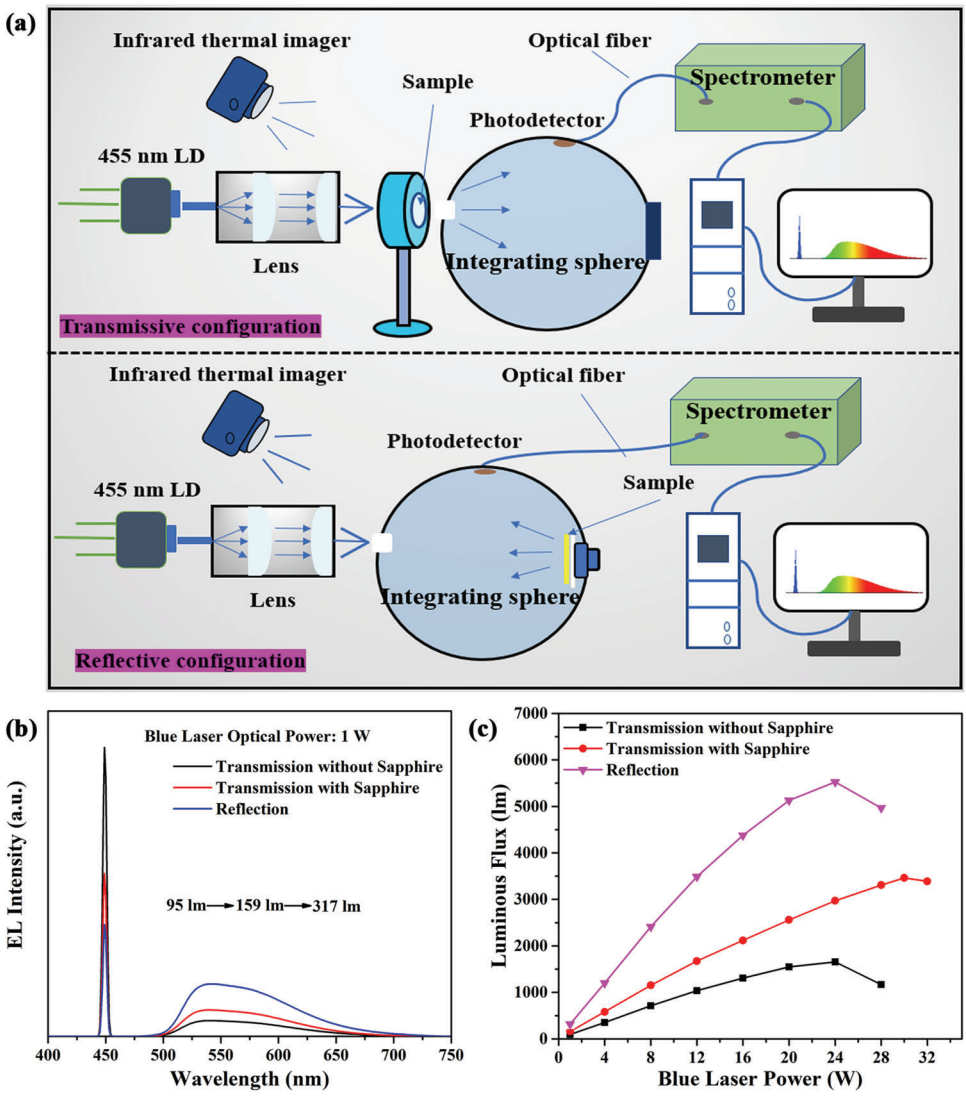

Figure 4. a) Schematical illustration of transmissive configuration and reflective configuration. b) Electroluminescence (EL) spectra and c) pumping power dependent luminous flux (LF) of YAG:Ce transparent ceramics (TC) sample under three different configurations.

cases has higher saturation threshold due to the heat dissipation of sapphire, the LF in reflection mode (5478 lm) is still significantly higher than that of transmission cases (1612 and 3458 lm). Therefore, the reflective light path configuration was chosen in the following section.

The CASN:Eu content was adjusted to optimize the final luminescent properties of CASN:Eu PiGF–YAG:Ce TC. As shown in **Figure 5**a, with CASN:Eu added, the proportion of red emissive component is effectively compensated. Figure 5b–f shows the changes of the measured/calculated LF, LE, CCT, CRI, and color coordinates for the CASN:Eu PiGF–YAG:Ce TC with different glass powder to CASN:Eu phosphor (GtC) ratios in dependence of the incident power density. As expected, because of the reabsorption effect and the nonradiative transitions, the maximum LF and LE of CASN:Eu PiGF–YAG:Ce TC are reduced compared with that of YAG:Ce TC.[23] Meanwhile, the fluorescence decay times of CASN:Eu is in the order of microseconds, and in each duration more electrons will stay in the excited state and are more likely to get pumped to the conduction band of the host or lead to ground-state depletion, which results in lower threshold of luminescence saturation.[24] It is expected that this problem can be solved within the development of red laser phosphors, which is not within the scope of this study.

When the CASN:Eu content is reduced, the saturation threshold first increases and then decreases (Figure 5b,c). The first increase is consistent with the result that the lesser absorbing centers for blue laser lead to the smaller amplitude variation of surface temperature as input laser power increases, since there are fewer nonradiative loss in color converters (Figure S12, Supporting Information).[1b] The subsequent decrease may be caused by the reduction in thermal conductivity, considering that glass is not a good conductor of heat compared with phosphors.[2c] Correspondingly, the amplitude of surface temperature variation dependent on power density becomes larger (Figure S12, Supporting Information). By the use of TC as the substrate via the strategy of "ceramic + glass ceramic film," the thermal

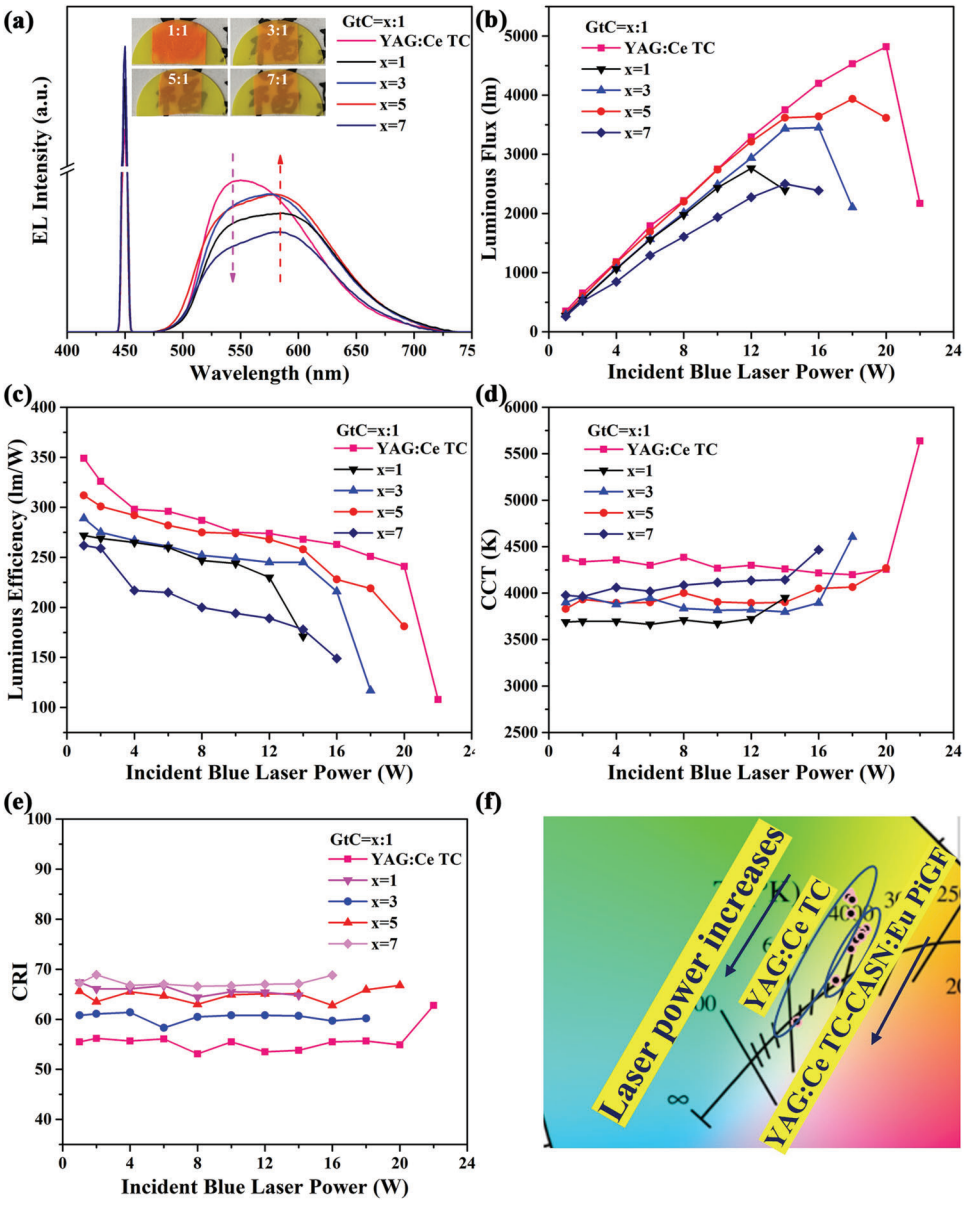

Figure 5. a) Luminescent spectra of CASN:Eu PiGF–YAG:Ce transparent ceramics (TC) (thickness: 0.40 mm) with different weight ratios of glass powder to CASN:Eu phosphor (GtC) upon 12 W blue laser excitation. Insets are photographs of the composite samples. The input power density dependent b) luminous flux (LF), c) luminous efficacy (LE), d) correlated color temperature (CCT), e) color rendering index (CRI), and f) color coordinates for the CASN:Eu PiGF–YAG:Ce TC (thickness: 0.40 mm) with different GtC upon blue laser driven.

conductivity of developed composite can be up to ≈10.33 W m^{-1} K^{-1} (Equation S1, Supporting Information), which is comparable to that of phosphor ceramics (e.g., LuAG:Ce^{3+} and CASN:Eu^{2+}, Table 1). The surface temperature at luminescence saturation is also similar to that of reported luminescence TC.[12b] It is also found that the surface temperature stabilized at about 240 °C when CASN:Eu PiGF–YAG:Ce TC was saturated, and the corresponding integrated luminescence intensity of YAG:Ce TC and CASN:Eu PiGF can retain 84% and 77%, respectively (Figures S6 and S9, Supporting Information). It seems that thermal quenching cannot induce luminescence saturation independently, and optical quenching caused by electron depletion of ground state and/or nonlinear upconversion processes in excited state also plays an indispensable role, which will be discussed later.[24] Meanwhile, due to the compensation of red-light band from CASN:Eu PiGF, the chromaticity gets warmer (CCT decreases), and the CRI increases significantly (Figure 5d,e). The chromaticity variation reflects the proportion of the converted yellow/red light to the excited blue light, accompanied with the photometric variation. As the pumping power density increases, the increase rate of yellow/red emission cannot keep up with that of blue laser light, and the color coordinates deviate toward blue region, while the color coordinates of CASN:Eu PiGF–YAG:Ce TC are always located near the Planckian locus trajectory (Figure 5f). The

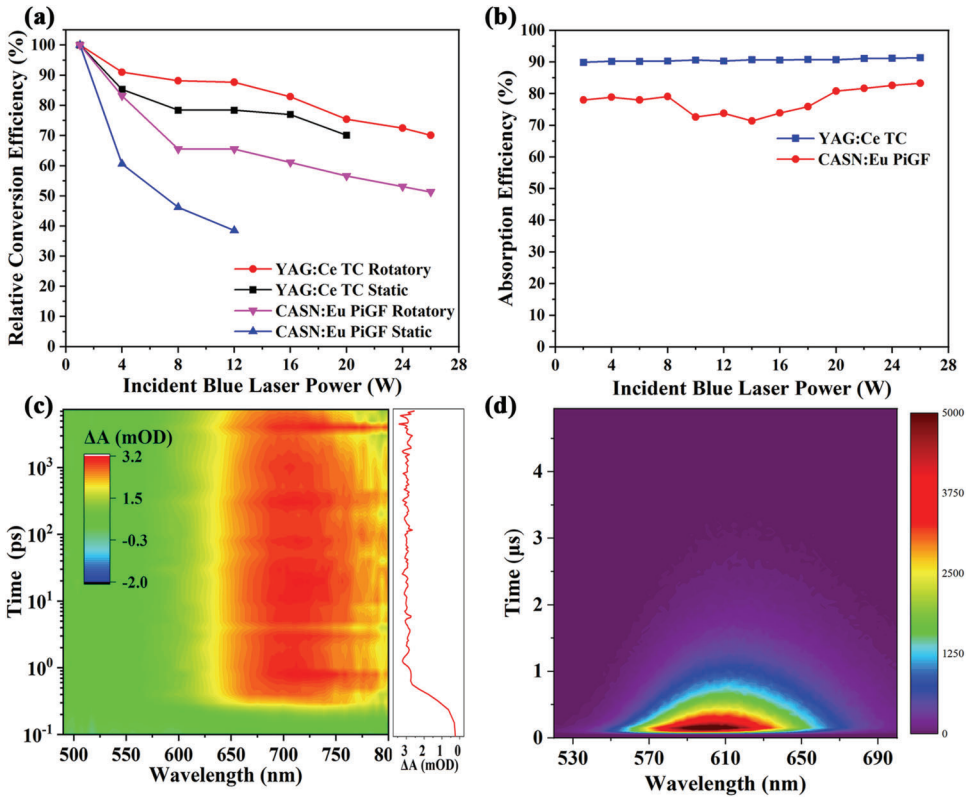

Figure 6. a) P_{in} dependent conversion efficiency (CE) variations for YAG:Ce transparent ceramics (TC) and CASN:Eu PiGF in the static and rotatory excitation modes. b) P_{in} dependent absorption efficiencies of the YAG:Ce TC and CASN:Eu PiGF under reflective-rotatory mode. c) Contour plot of the *fs* transient absorption (TA) spectra upon photoexcitation at 450 nm with a time window from 0 to 8000 ps of YAG:Ce TC. The right panel in (c) shows the corresponding ultrafast dynamics curve probed at 718 nm. d) Time-resolved photoluminescence spectra (TRPL) spectra of CASN:Eu PiGF under laser excitation.

optimized CASN:Eu PiGF–YAG:Ce TC shows a high LF of 3935 lm, a high LE of 218 lm W^{-1}, a good CRI of 65.9 (in comparison, CRI is 55.7 for YAG:Ce TC), and a CCT of 4055 K, upon 18 W blue LD driven when luminescence saturation. It is believed that, when coupling with cyan-green emitting phosphors, the CRI can be further improved due to the balanced spectral distribution over entire visible region.

A series of experiments on YAG:Ce TC and CASN:Eu PiGF were conducted to explore the mechanism of luminescence saturation. The rotatory excitation mode can effectively control the temperature variation and eliminate the thermal saturation effect. In other words, optical excitation intensity quenching is the only influential factor to the conversion efficiency (CE) drop at elevated incident blue laser power (P_{in}) on this condition. It is found that through plotting P_{in}–CE relationship in both static excitation mode and rotatory excitation mode, the CE of YAG:Ce TC and CASN:Eu PiGF always decreases at an elevated P_{in} (**Figure 6**a). The relative CE drop of static mode is significantly higher than that of rotatory mode, based on which the contribution of thermal saturation and optical saturation in luminescence saturation can be evaluated.[1b] At the saturated P_{in} (20 W) of YAG:Ce TC, CE drop relative to the initial CE at low power density is 29.9% under static mode, while the data is 24.6% under rotatory mode, and the contributions from thermal saturation and optical saturation are 18% and 82%, respectively. Similarly, at the saturated P_{in} for CASN:Eu PiGF, the relative CE drop is 61.5%, and the CE drop (majorly induced by optical saturation) is 34.5%, converting to 44% contribution of thermal saturation and 56% contribution of optical saturation. Based on these results, it can be found that thermal-optical quenching induced by high-photon flux irradiation plays an important role in the luminescence saturation of CASN:Eu PiGF–YAG:Ce TC composite. The luminescence saturation is caused by the combined action of thermal quenching and optical excitation intensity quenching upon high-power blue laser driven.

As for the cause of optical quenching, the effect of ground state depletion (GSD) (there are not sufficient electrons in the ground state for pumping) can be excluded by almost invariable absorption efficiency (<10%), which does not conform to the characteristics of GSD (Figure 6b).[24a] Probing the femtosecond transient absorption (fs TA) spectra of YAG:Ce TC upon photoexcitation at 450 nm, it can be found that the absorption band is mainly in the red spectral region of 620–800 nm, overlapping with its emission spectra, which indicates that the converted photons can be reabsorbed (Figure 6c and Figure S13, Supporting Information). On the other hand, the decay time of excited-state absorption even exceeds the detection limit (8000 ps), which makes the excited-state absorption be medium for the storage and transport of electrons, considering that the electrons are able to availably stay in the excited state. Therefore, the energy upconversion

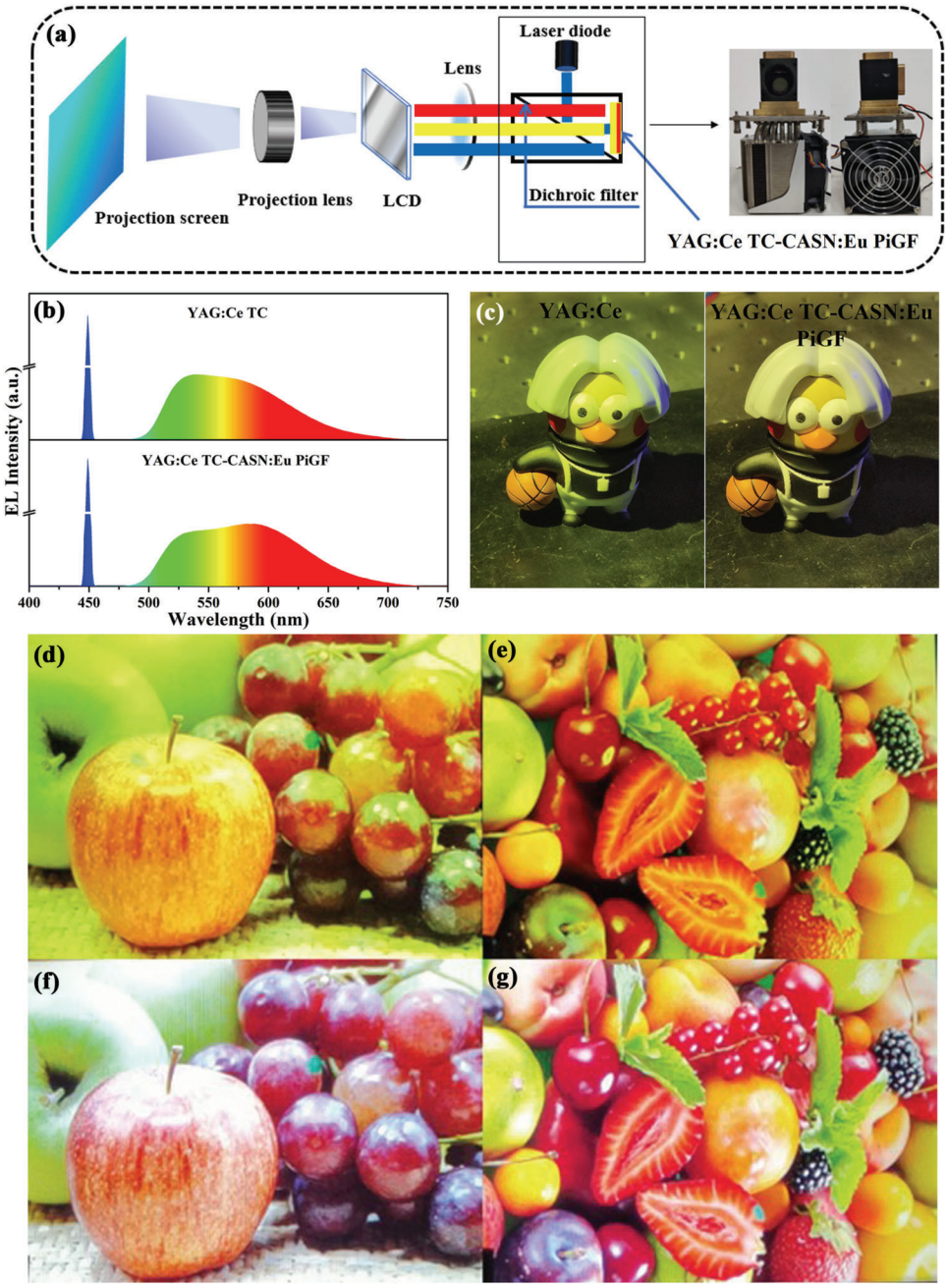

Figure 7. a) Illustration of light path for the CASN:Eu PiGF–YAG:Ce transparent ceramics (TC) converted laser-driven projection system. b) Electroluminescence (EL) spectra of YAG:Ce TC and CASN:Eu PiGF–YAG:Ce TC. c) Demonstration experiment of illuminating a toy driven by lighting sources based on YAG:Ce TC and CASN:Eu PiGF–YAG:Ce TC, respectively. Projection display performance of d,e) YAG:Ce TC converted laser-driven projector and f,g) CASN:Eu PiGF–YAG:Ce TC converted laser-driven projector.

dominated by second-order nonlinear processes (containing excited state absorption upconversion ESA for a single active ion and Auger energy transfer upconversion ETU for two neighboring active ions) via pumping electrons to conduction band is very likely to happean.[24] The time-resolved PL spectra (TRPL) of CASN:Eu PiGF depicts that the TRPL are red-shifted with delay time because of the energy transfer from the high-energy Eu^{2+} to the low-energy Eu^{2+}, which indicates the strong interaction between the Eu^{2+} of CASN:Eu PiGF (Figure 6d and Figure S14, Supporting Information). The probability of optical quenching via energy upconversion dominated by second-order nonlinear processes is highly plausible.

Finally, YAG:Ce TC/CASN:Eu PiGF–YAG:Ce TC -converted laser-driven projection system was built to directly illustrate the application potential of developed composite material. The light path of projection system is shown in **Figure 7**a. The blue laser was located 10 cm in front of the dichroic filter with a short focal lens on the other side. The LCD screen programming with

specific picture was located 15 cm in front of the dichroic mirror where the converted light exits. Figure 7b,c displays EL spectra and luminescent photographs of the constructed lighting source based on YAG:Ce TC and CASN:Eu PiGF–YAG:Ce TC under blue LD excitation respectively, and the chromaticity difference can be intuitively discerned by the naked eyes. The former shows yellowish color and a low CRI of 55.5, while the latter shows warm white with high CRI of 65.6. Furthermore, in terms of projection display, due to the brighter separated light of red light from balanced-spectrum composite than traditional YAG:Ce TC, more details and more vivid and saturated color can be observed through the use of CASN:Eu PiGF–YAG:Ce TC especially for the red objects (Figure 7d–g).

By reason of the broadband spectra, the color gamut of the fabricated lighting source cannot be measured directly; instead, it will be entirely determined by the commercial color filters (Figure S15, Supporting Information). Thereupon, there is a very limited difference in color gamut ranges between CASN:Eu PiGF–YAG:Ce TC (77% NTSC) and YAG:Ce TC (76% NTSC) after passing through the commercial RGB color filters (Figure S16, Supporting Information). It is believed that when coupled with more advanced filters, the color gamut can be well improved. Meanwhile, the corresponding display effect is verified by the experiment based on single LCD backlight technology. Because of the more balanced separated light of blue, red, and green light from designed composite than traditional YAG:Ce TC, the present composite would also illustrate the promising application in projector display with more complex tri-LCD or tri-DMD.

3. Conclusion

In summary, we have proposed a new material architecture design of "ceramic + glass ceramic film" to develop color converters potentially applicable to high brightness laser-driven projection display for the first time, which can effectively solve the notorious issue of deficient red emissive component upon the irradiation of blue LD. With this design, a novel CASN:Eu PiGF–YAG:Ce TC has been developed, and its microstructure and spectroscopic performance have been systematically studied. Based on the luminescence properties upon blue laser excitation, it can be shown that the photometric and colorimetric parameters of reflection light path configuration are the best. The optimized CASN:Eu PiGF–YAG:Ce TC can produce high-quality white light, with a maximum LF of 3935 lm, LE of 218 lm W^{-1}, CRI of 65.9, and warm CCT of 4055 K. Probing into luminescence saturation mechanism, the thermal-optical quenching plays an important role, and the second-order nonlinear process is believed responsible for the optical saturation. We have conducted a series of laser-driven projection system to evaluate the application feasibility of developed materials. Compared with traditional YAG:Ce TC converted laser-driven projector, the demo based on CASN:Eu PiGF–YAG:Ce TC shows better display effect. This study demonstrates an effective material architecture design to simultaneously achieve the balanced-spectrum properties and strong heat dissipation, and proposes an admirable composite material for high brightness laser-driven projection display.

Supporting Information

Supporting Information is available from the Wiley Online Library or from the author.

Acknowledgements

S.X.L. and S.L.J. contributed equally to this work. This research was supported by National Key Research and Development Program of China (2021YFB3500503), National Natural Science Foundation of China (52272141, 51972060, 12074068, 52102159, and 22103013), Fujian Science and Technology Innovation Laboratory for Optoelectronic Information of China (2021ZZ126), and Natural Science Foundation of Fujian Province (2022J05091, 2020J02017, 2021J06021, 2021J01190, 2020J01931, and 2020H0026).

Conflict of Interest

The authors declare no conflict of interest.

Data Availability Statement

Research data are not shared.

Keywords

ceramics, color converters, glass ceramics, laser-driven projection displays, luminescent materials

Received: July 6, 2023
Revised: September 21, 2023
Published online:

[1] a) S. Li, L. Wang, N. Hirosaki, R. J. Xie, *Laser Photonics Rev.* **2018**, *12*, 1800173; b) S. Lin, H. Lin, Q. Huang, H. Yang, B. Wang, P. Wang, P. Sui, J. Xu, Y. Cheng, Y. Wang, *Laser Photonics Rev.* **2022**, *16*, 2200523; c) H. Liao, M. Zhao, Y. Zhou, M. S. Molokeev, Q. Liu, Q. Zhang, Z. Xia, *Adv. Funct. Mater.* **2019**, *29*, 1901988; d) X. Li, Y. Wu, S. Zhang, B. Cai, Y. Gu, J. Song, H. Zeng, *Adv. Funct. Mater.* **2016**, *26*, 2435; e) S. Chen, J. Lin, S. Zheng, Y. Zheng, D. Chen, *Adv. Funct. Mater.* **2023**, *13*, 2213442; f) T. Deng, D. Halmurat, Z. Shen, T. Yan, S. Li, R. J. Xie, *Laser Photonics Rev.* **2023**, *17*, 2300240.

[2] a) Y. Zhou, C. Yu, E. Song, Y. Wang, H. Ming, Z. Xia, Q. Zhang, *Adv. Opt. Mater.* **2020**, *8*, 2000976; b) Q. Huang, P. Sui, F. Huang, H. Lin, B. Wang, S. Lin, P. Wang, J. Xu, Y. Cheng, Y. Wang, *Laser Photonics Rev.* **2022**, *16*, 2200040; c) S. Lin, H. Lin, P. Wang, P. Sui, H. Yang, J. Xu, Y. Cheng, Y. Wang, *J. Mater. Chem. C* **2023**, *11*, 1530.

[3] a) X. Yue, J. Xu, H. Lin, S. Lin, R. Li, B. Wang, Q. Huang, P. Wang, P. Sui, Y. Cheng, *Laser Photonics Rev.* **2021**, *15*, 2100317; b) J. Li, D. Zhou, Y. Liu, Y. Chen, J. Chen, Y. Yang, Y. Gao, J. Qiu, *ACS Appl. Mater. Interfaces* **2023**, *15*, 22219; c) P. Sui, H. Lin, Y. Lin, S. Lin, J. Huang, J. Xu, Y. Cheng, Y. S. Wang, *Opt. Lett.* **2022**, *47*, 3455.

[4] a) S. Lin, H. Lin, G. Chen, B. Wang, X. Yue, Q. Huang, J. Xu, Y. Cheng, Y. Wang, *Laser Photonics Rev.* **2021**, *15*, 2100044; b) S. Liao, Z. Yang, J. Lin, S. Wang, J. Zhu, S. Chen, F. Huang, Y. Zheng, D. Chen, *Adv. Funct. Mater.* **2023**, *33*, 2210558; c) G. Li, Q. Pan, Z. Zhou, R. Gu, H. Zhang, X. Huang, G. Dong, X. Xiao, *Adv. Opt. Mater.* **2023**, *11*, 2203028.

[5] a) T. Kaji, H. Morita, Y. Maeda, C. Wall, D. Chercka, N. Krasteva, I. Kobayashi, *SID Int. Symp. Dig. Tech. Pap.* **2020**, *51*, 1240; b) F. Hu, C. Zhang, Z. Guo, C. Chen, Y. Li, *SID Int. Symp. Dig. Tech. Pap.* **2020**, *51*, 1234.

[6] a) Q. Li, W. Xiao, D. Zhang, D. Wang, G. Zheng, J. Qiu, *Laser Photonics Rev.* **2022**, *16*, 2200553; b) Y. Li, Y. F. Liu, Z. Luo, Z. Liu, S. Hanson, C. Pang, H. Lin, H. Qin, J. Jiang, *Ceram. Int.* **2023**, *49*, 24703.
[7] Y. Pan, F. Zhu, J. Fan, J. Tao, X. Lin, F. Wang, L. Shi, *Polymers* **2018**, *10*, 195.
[8] J. Xu, A. Thorseth, C. Xu, A. Krasnoshchoka, M. Rosendal, C. Dam-Hansen, B. Du, Y. Gong, O. B. Jensen, *J. Lumin.* **2019**, *212*, 279.
[9] a) R. Zhang, H. Lin, Y. Yu, D. Chen, J. Xu, Y. Wang, *Laser Photonics Rev.* **2014**, *8*, 158; b) D. Zhang, W. Xiao, C. Liu, X. Liu, J. Ren, B. Xu, J. Qiu, *Nat. Commun.* **2020**, *11*, 1;. c) J. Yu, S. Si, Y. Liu, X. Zhang, Y. Cho, Z. Tian, R. Xie, H. Zhang, Y. Li, J. Wang, *J. Mater. Chem. C* **2018**, *6*, 8212.
[10] a) P. Zheng, S. Li, R. Wei, L. Wang, T. L. Zhou, Y. R. Xu, T. Takeda, N. Hirosaki, R. J. Xie, *Laser Photonics Rev.* **2019**, *13*, 1900147; b) P. Zheng, S. Li, L. Wang, T.-L. Zhou, S. You, T. Takeda, N. Hirosaki, R.-J. Xie, *ACS Appl. Mater. Interfaces* **2018**, *10*, 14930; c) H. Wu, G.-H. Pan, Z. Hao, L. Zhang, H. Wu, J. Zhang, *J. Mater. Chem. C* **2021**, *9*, 12342.
[11] Q. Yao, P. Hu, P. Sun, M. Liu, R. Dong, K. Chao, Y. Liu, J. Jiang, H. Jiang, *Adv. Mater.* **2020**, *32*, 1907888.
[12] a) S. Liu, P. Sun, Y. Liu, T. Zhou, S. Li, R.-J. Xie, X. Xu, R. Dong, J. Jiang, H. Jiang, *ACS Appl. Mater. Interfaces* **2018**, *11*, 2130; b) Y. Xu, S. Li, P. Zheng, L. Wang, S. You, T. Takeda, N. Hirosaki, R.-J. Xie, *J. Mater. Chem. C* **2019**, *7*, 11449.
[13] a) S. Feng, H. Qin, G. Wu, H. Jiang, J. Zhao, Y. Liu, Z. Luo, J. Qiao, J. Jiang, *J. Eur. Ceram. Soc.* **2017**, *37*, 3403; b) H. Yang, Y.-S. Kim, *J. Lumin.* **2008**, *128*, 1570.
[14] J. Wang, X. Tang, P. Zheng, S. Li, T. Zhou, R.-J. Xie, *J. Mater. Chem. C* **2019**, *7*, 3901.
[15] K. Li, Y. Shi, F. Jia, C. Price, Y. Gong, J. Huang, N. Copner, H. Cao, L. Yang, S. Chen, *IEEE Photonic Technol. Lett.* **2018**, *30*, 939.
[16] S. Li, D. Tang, Z. Tian, X. Liu, T. Takeda, N. Hirosaki, F. Xu, Z. Huang, R.-J. Xie, *J. Mater. Chem. C* **2017**, *5*, 1042.
[17] L. Wang, H. Yang, Y. Zhang, Y. Liang, J. Zhang, E. Mei, F. Xu, J. Long, P. Yu, W. Xiang, *J. Alloys Compd.* **2022**, *892*, 161882.
[18] J. Zhang, H. Yang, Y. Zhang, X. Liu, Y. Zhang, Y. Liang, H. Li, B. Ma, X. Liang, W. Xiang, *Appl. Phys. Lett.* **2021**, *119*, 023301.
[19] Y. Zhang, Z. Zhang, X. Liu, G. Shao, L. Shen, J. Liu, W. Xiang, X. Liang, *Chem. Eng. J.* **2020**, *401*, 125983.
[20] Q.-Q. Zhu, X.-J. Wang, L. Wang, N. Hirosaki, T. Nishimura, Z.-F. Tian, Q. Li, Y.-Z. Xu, X. Xu, R.-J. Xie, *J. Mater. Chem. C* **2015**, *3*, 10761.
[21] T. Hu, L. Ning, Y. Gao, J. Qiao, E. Song, Z. Chen, Y. Zhou, J. Wang, M. S. Molokeev, X. Ke, *Light: Sci. Appl.* **2021**, *10*, 1.
[22] Z. Liu, X. Yu, Q. Peng, X. Zhu, J. Xiao, J. Xu, S. Jiang, J. Qiu, X. Xu, *Adv. Funct. Mater.* **2023**, *33*, 2214497.
[23] Q. Huang, H. Lin, B. Wang, S. Lin, P. Wang, P. Sui, J. Xu, Y. Cheng, Y. Wang, *J. Adv. Ceram.* **2022**, *11*, 862.
[24] a) P. Zheng, S. Li, T. Takeda, J. Xu, K. Takahashi, R. Tian, R. Wei, L. Wang, T.-L. Zhou, N. Hirosaki, *Acta Mater.* **2021**, *209*, 116813; b) A. Lenef, M. Raukas, J. Wang, C. Li, *ECS J. Solid State Sci. Technol.* **2019**, *9*, 016019; c) O. B. Shchekin, P. J. Schmidt, F. Jin, N. Lawrence, K. J. Vampola, H. Bechtel, D. R. Chamberlin, R. Mueller-Mach, G. O. Mueller, *Phys. Status Solidi RRL* **2016**, *10*, 310.